Radion Model for the Di-photon Signal at 750 GeV: arXiv:1512.05771

Collaborators: Aqeel Ahmed (NCP, Islamabad & Warsaw U.), Barry M. Dillon (Sussex U.), Bohdan Grzadkowski (Warsaw U.), John F. Gunion (UC, Davis), Yun Jiang (Bohr Inst.).

Jack Gunion
U.C. Davis

SUSY2016, July 5, 2016

We have come to a crossroads. The existence of a SM-like Higgs constrains all directions of exploration.

Motivational Issues

- There is a rather SM-like Higgs boson at $m_h = 125$ GeV.
- There is no sign of supersymmetry.
- There is an increasingly convincing excess of di-photon events at $m_{\gamma\gamma} \sim 750$ GeV.
- Maybe it is time to look at alternative models in which there is **no hierarchy problem** and the two observed states are present with the observed cross sections and characeristics.

The Randall Sundrum two-brane model fits the bill. In this model one places the SM, including its Higgs sector, into the context of a 5th (extra) dimension.

Two options:

A: The 750 GeV state is the first excited KK mode of the graviton with mass $m_1^{\rm KK}$.

B: The 750 GeV state is mainly (but not entirely) the radion, ϕ, of the model, where the radion is the quantum fluctuation associated with the separation of the two branes.

Two more options: do SM particles propagate in the bulk or are they localized on the IR (TeV) brane?

1. Localize on the brane:

   The gluon (and other SM particles) do not propagate in the bulk and hence there are no excited states of the gluon (or any other SM particle). This means that there are no collider bounds on the excited states (KK modes) of the SM particles since they don't exist.

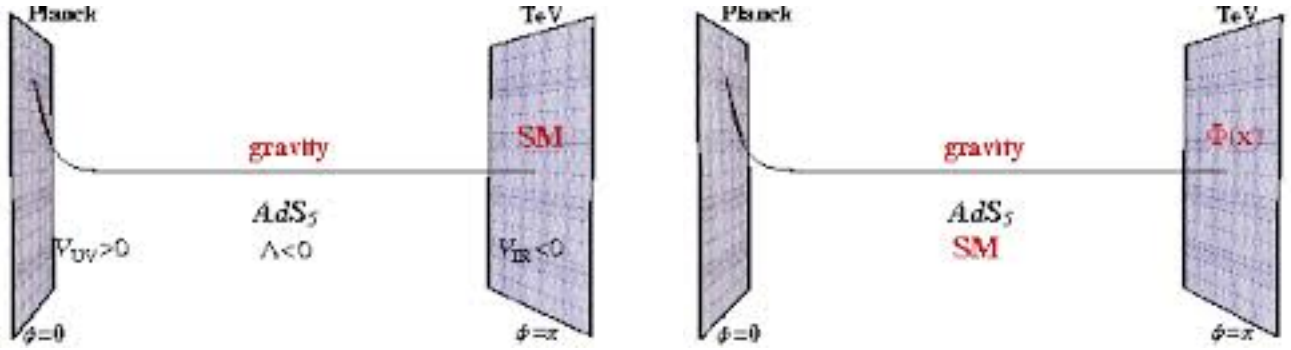

Figure 1: The two RS brane pictures.

2. Allow the gauge bosons and possibly other SM particles to propagate in the bulk.

   The excited state of immediate importance is the first excitation of the gluon with mass m_1^g. In this case, collider data already imply $m_1^g > 3$ TeV.

- Option A (KK graviton) has been considered by Giddings/Zhang (1602.02793) and Hewett/Rizzo (1603.08250).
  - The G&Z model has basically one parameter Λ that determines everything once $m_1^{\rm KK} = 750$ GeV is imposed.
  - $\Lambda \sim 60$ TeV and small $k/M_{\rm Pl}$ are required in order to fit the di-photon signal.
  - But, other final states are predicted to have very significant rates. The most worrisome are the $e^+e^-, \mu^+\mu^-$ final states, predictions for which are only very marginally consistent with existing 8 TeV limits (at 95% CL) basically because $B(G_1 \to e^+e^-) = 0.5 B(G_1 \to \gamma\gamma)$. 13 TeV data will confirm or exclude soon. H&R include BLKT (brane-localized kinetic terms) to escape this problem.

- Option B (Radion) is our choice: arXiv:1512.05771
  - We claim the most (and maybe only) natural interpretation of the 750 GeV state is a radion. It really works very well provided gauge bosons propagate in the bulk – option 2..
  - In particular, we will see that if the gluon propagates in the bulk then the KK graviton cannot be as light as 750 GeV.

Although dark matter is not present in the simplest incarnation of the RS Higgs-radion approach, it is easily added, for example by adding an extra (stable) singlet to the simplest one-doublet Higgs sector of the model.

Basics of the Model

- RS metric:

$$ds^2 = e^{-2kb_0|y|}\eta_{\mu\nu}dx^\mu dx^\nu - b_0^2 dy^2, \tag{1}$$

  - k is the curvature of the 5D geometry,
  - b_0 is a length parameter for the 5th dimension, and $-1/2 \leq y \leq 1/2$.
  - $\frac{1}{2}kb_0 \sim 35$, for the RS model to constitute a full solution to the hierarchy problem.
  - The fluctuation of the 55-component associated with b_0 is the radion, $\phi_0(x)$. The VEV of ϕ_0 is denoted Λ_ϕ.

- Critical parameter relations:

  - $m_1^{\rm KK} = x_1^{KK}\frac{k}{M_{\rm Pl}}\frac{\Lambda_\phi}{\sqrt{6}}$, where $x_1^{KK} = 3.83$ (Note: $x_2^{KK} \sim 7$).
  - $m_1^g = x_1^g\frac{k}{M_{\rm Pl}}\frac{\Lambda_\phi}{\sqrt{6}}$ $(\sim \frac{k}{M_{\rm Pl}}\Lambda_\phi)$, where $x_1^g = 2.45$, implying $m_1^{\rm KK} \simeq 1.55 m_1^g$.
  - Collider data limit of $m_1^g > 3$ TeV, implies $m_1^{\rm KK} > 4.6$ TeV.
    This can be avoided at the price of including brane kinetic terms for gauge fields and gravity localized on the "visible" (IR) brane. Without this, only the radion interpretation of the 750 GeV resonance is viable. $\Rightarrow$ The natural choice.

- For the radion interpretation of the 750 GeV state it is critical to include a Higgs-gravity coupling, $\xi\mathcal{R}_4 H^\dagger H$ (localized on the IR brane), where

  ξ is a dimensionless parameter and

  $\mathcal{R}_4$ is the four-dimensional (4D) Ricci scalar coming from the induced metric on the IR brane.

  This results in the following 4D effective Lagrangian for the scalar sector,

$$\mathcal{L}_{\rm eff} = \frac{1}{2}(\partial_\mu\phi_0)^2 - \frac{1}{2}m_{\phi_0}^2\phi_0^2 - 6\xi\Omega\Box\Omega H^\dagger H + |D_\mu H|^2 - \Omega^4 V(H), \qquad (2)$$

  where ϕ_0 is the (unmixed) radion field and m_{ϕ_0} its bare mass. Above, $\Omega(\phi_0) \equiv 1 - \ell\phi_0/v_0$, where

$$\ell \equiv \frac{v_0}{\Lambda_\phi} \qquad (3)$$

  with $v_0 = 246$ GeV and $\Lambda_\phi \equiv \sqrt{6}M_{\rm Pl}e^{-kb_0/2}$ is the vacuum expectation value (VEV) of the radion field.

  As we will show below, phenomenological constraints make it difficult to accommodate $\Lambda_\phi \lesssim 1.5$ TeV, implying that ℓ is limited to $\ell \lesssim 1/6$.

- At the quadratic level, the above yields

$$\mathcal{L}^{(2)}_{\rm eff} = -\frac{1}{2}(1+6\xi\ell^2)\phi_0\Box\phi_0 - \frac{1}{2}m^2_{\phi_0}\phi_0^2 + 6\xi\ell h_0\Box\phi_0 - \frac{1}{2}h_0\Box h_0 - \frac{1}{2}m^2_{h_0}h_0^2, \quad (4)$$

where h_0 is the neutral scalar of the Higgs doublet H, and $m_{h_0} \equiv \sqrt{2\lambda}v_0$ is the bare Higgs mass. In the above Lagrangian, the ξ term that mixes the Higgs and the radion can be removed by rotating the scalar fields into the mass eigenstate basis,

$$\begin{pmatrix}\phi_0\\ h_0\end{pmatrix} = \begin{pmatrix}-a & -b\\ c & d\end{pmatrix}\begin{pmatrix}\phi\\ h\end{pmatrix}, \quad (5)$$

where $a = -\cos\theta/Z$, $b = \sin\theta/Z$, $c = \sin\theta + t\cos\theta$ and $d = \cos\theta - t\sin\theta$, with $t \equiv 6\xi\ell/Z$, $Z^2 \equiv 1 + 6\xi\ell^2(1-6\xi)$ and

$$\tan 2\theta = \frac{12\xi\ell Z m^2_{h_0}}{m^2_{\phi_0} - m^2_{h_0}(Z^2 - 36\xi^2\ell^2)}. \quad (6)$$

Given that $\ell \lesssim 1/6$ for the $\Lambda_\phi \gtrsim 1.5$ TeV range of interest and that we will focus on ξ values near the $\xi = 1/6$ conformal limit, it is legitimate to expand Eq. (6) in

powers of ℓ and express the result in terms of the physical mass parameters, m_h and m_ϕ:

$$\tan 2\theta = \frac{12\xi\ell m_{h_0}^2}{Z(m_\phi^2 + m_h^2 - 2m_{h_0}^2)} \simeq 12\xi\ell\left(\frac{m_h}{m_\phi}\right)^2\left[1 - 3\xi(1-6\xi)\ell^2\right] + \cdots, \quad (7)$$

where the ellipsis stands for terms which are quite small for $m_\phi = 750$ GeV and $\Lambda_\phi \gtrsim 1.5$ TeV. For $\xi = 1/6$ and $\ell \lesssim 1/6$ one obtains $\theta \simeq \ell(m_h/m_\phi)^2 \lesssim (1/6)^3$.

- IMPORTANT: relation between m_1^g (1st gluonic KK excitation), $\langle\phi_0\rangle = \Lambda_\phi$ and the curvature ratio $k/M_{\rm Pl}$:

$$m_1^g = \frac{x_1^g}{\sqrt{6}}\frac{k}{M_{\rm Pl}}\Lambda_\phi \simeq \frac{k}{M_{\rm Pl}}\Lambda_\phi, \quad (8)$$

where $x_1^g \simeq 2.45$ is the 1st zero of an appropriate Bessel function. This relation is depicted in the following figure.

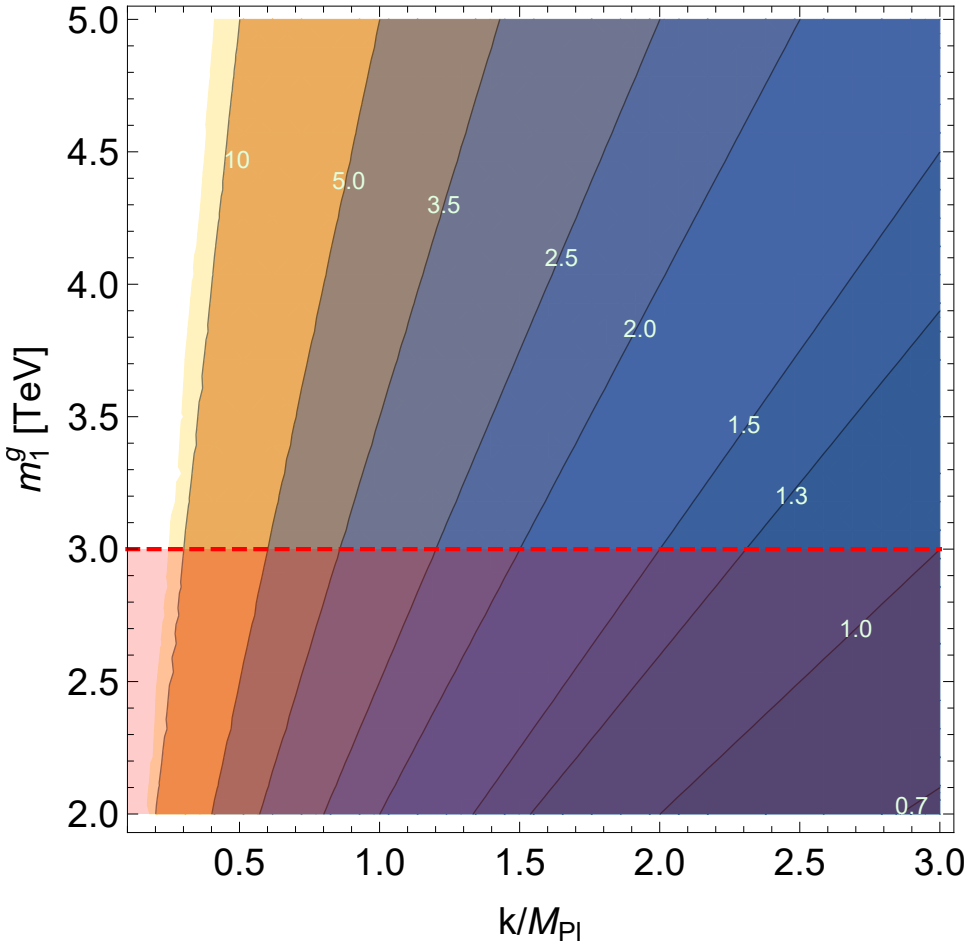

Figure 2: Correlation between m_1^g and $k/M_{\rm Pl}$ for different contours of Λ_ϕ (in TeV). The region below $m_1^g = 3$ TeV (dashed-red line) is excluded by the EWPO and direct collider limits. We will need $\Lambda_\phi \lesssim 2.5$ TeV which implies $k/M_{\rm Pl} \gtrsim 1$. $\Lambda_\phi = 1.5$ TeV requires $k/M_{\rm Pl} = 2$ (3) for $m_1^g = 3$ TeV (5 TeV). Originally, $k/M_{\rm Pl}$ values < 1 seemed best motivated; however, more recently (Agashe et. al., [hep-ph/0308036]) show that $k/M_{\rm Pl}$ values > 1 are equally ok, with $k/M_{\rm Pl}$ as large as 3 possible without invoking quantum gravity related issues.

- **Particle "locations":**
  - The Higgs, t_L, t_R and b_L will be placed on the IR brane $\Rightarrow$ heavy t natural.
  - We want to place all gauge bosons in the bulk.
    * In the case of the g and γ this is required in order to have enhanced gg and $\gamma\gamma$ couplings.
    * But, if the W and Z are in the bulk, EWPO constraints naively imply $m_1^g > 10$ TeV, which implies too large a value for Λ_ϕ to obtain the observed di-photon cross-section.
    * However, by introducing a local custodial symmetry of $SU(2)_L \times SU(2)_R \times U(1)_X$ (where the $SU(2)_R \times U(1)_X$ fields are broken to $U(1)_Y$ on the UV brane, such that $Y = T_R^3 + X$) then it is possible for m_1^g to have mass as low as $m_1^g \sim 3$ to 5 TeV.
      This is required for the model to have low enough Λ_ϕ, *i.e.* $\Lambda_\phi \lesssim 2.5$ TeV (see Fig. 2) so as to reproduce the observed di-photon cross-section.

- **Radion couplings:** In the following figure, the $4\pi/(\alpha_{(s)} k b_0)$ for the $\gamma\gamma, gg$ couplings and the κ_V terms and non-SM tensor structures in the WW and ZZ vertices are all due to the vector bosons being present in the bulk. Note the anomalous coupling terms for WW, ZZ. These are often neglected relative to M_V^2 terms, but these latter will be quite suppressed when the $\gamma\gamma$ signal is maximized.

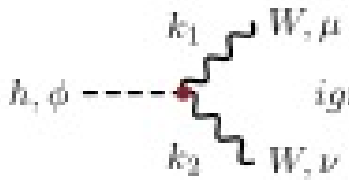

$$ig m_W \left(g_{h,\phi} - g^r_{h,\phi}\kappa_W\right)\left[\eta^{\mu\nu} - 2g^W_{h,\phi}\left(\eta^{\mu\nu}k_1\cdot k_2 - k_1^\nu k_2^\mu\right)\right]$$

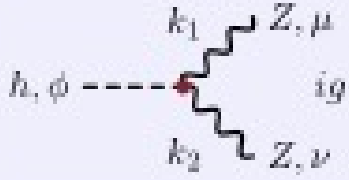

$$ig\frac{m_Z}{\cos\theta_W}\left(g_{h,\phi} - g^r_{h,\phi}\kappa_Z\right)\left[\eta^{\mu\nu} - 2g^Z_{h,\phi}\left(\eta^{\mu\nu}k_1\cdot k_2 - k_1^\nu k_2^\mu\right)\right]$$

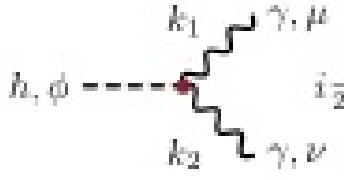

$$i\frac{\alpha}{2\pi v_0}\left[g^r_{h,\phi}\left(b_2 + b_Y + \frac{4\pi}{\alpha k b_0}\right) - g_{h,\phi}\textstyle\sum_i e_i^2 N_c^i F_i(\tau_i)\right]\left(\eta^{\mu\nu}k_1\cdot k_2 - k_1^\nu k_2^\mu\right)$$

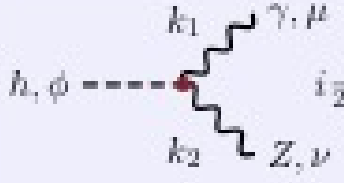

$$i\frac{\alpha}{2\pi v_0}\left[2g^r_{h,\phi}\left(\frac{b_2}{\tan\theta_W} - b_Y\tan\theta_W\right) - g_{h,\phi}\textstyle\sum_i e_i^2 N_c^i G_i(\tau_i)\right]\left(\eta^{\mu\nu}k_1\cdot k_2 - k_1^\nu k_2^\mu\right)$$

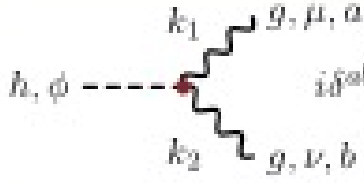

$$i\delta^{ab}\frac{\alpha_s}{4\pi v_0}\left[2g^r_{h,\phi}\left(b_3 + \frac{4\pi}{\alpha_s k b_0}\right) - g_{h,\phi}\textstyle\sum_i F_{1/2}(\tau_i)\right]\left(\eta^{\mu\nu}k_1\cdot k_2 - k_1^\nu k_2^\mu\right)$$

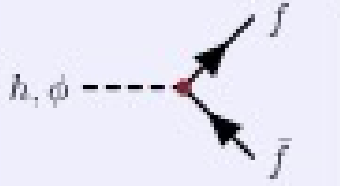

$$-i\frac{g}{2}\frac{m_f}{m_W}g_{h,\phi}$$

where $\quad g_h \equiv (d + \ell b), \quad g_\phi \equiv (c + \ell a), \quad g^r_h \equiv \ell b, \quad g^r_\phi \equiv \ell a,$

$$\kappa_V \equiv \frac{3m_V^2 k b_0}{2\Lambda_\phi^2 (k/M_{\rm Pl})^2}, \qquad g^V_{h,\phi} \equiv \frac{g^r_{h,\phi}}{(g_{h,\phi} - \kappa_V g^r_{h,\phi})m_V^2}\left(\frac{1}{2kb_0} + g_V^{\rm anom}\right)$$

$$g_W^{\rm anom} \equiv \frac{\alpha}{8\pi}\frac{b_2}{\sin^2\theta_W}, \qquad g_Z^{\rm anom} \equiv \frac{\alpha}{8\pi}\left(\frac{b_2}{\tan^2\theta_W} + b_Y\tan^2\theta_W\right)$$

$b_2 = 19/6, \quad b_Y = -41/6, \quad b_3 = 7, \qquad \theta_W$: Weinberg angle

Notes:

- The coupling of the radion to the trace of the energy momentum tensor and the propagation of all gauge bosons in the bulk imply that $\phi\gamma\gamma$, ϕgg, ϕWW, ϕZZ and $\phi Z\gamma$ all couplings have extra "anomalous" contributions with magnitude determined by the respective β functions.
- In addition, the g and γ couplings have $\frac{4\pi}{\alpha_s k b_0}$ and $\frac{4\pi}{\alpha k b_0}$ terms, respectively, added to the anomalous contributions.
  In the $\gamma\gamma$ case, the small size of α implies that this piece dominates the anomaly piece. Indeed, without this extra "bulk" piece the $\gamma\gamma$ signal rate could not be as large as that observed.
- As discussed below, the other pieces ($i.e.$ those proportional to g_ϕ) will be small for the choices of $\xi \sim 0.162$ of relevance, where the $t\bar{t}$, $b\bar{b}$ and hh couplings are nearly zero.
  $\Rightarrow$ at $\xi = 0.162$, gg will dominate and $\gamma\gamma$ will be big.

- **Coincident "zeroes".**

1. For the $t\bar{t}$, $b\bar{b}$ the coupling strength is:

$$g_\phi = \ell \left[6\xi \left(\frac{m_h}{m_\phi} \right)^2 + 6\xi - 1 \right] \simeq \ell \left(\frac{37}{6}\xi - 1 \right) \tag{9}$$

One finds $g_\phi = 0$ for $\xi \simeq 0.162162$. **At this point the gg and $\gamma\gamma$ couplings come entirely from the anomalous+bulk contributions**.

2. For the hh coupling one finds:

$$\frac{g_{\phi hh}\Lambda_\phi}{m_\phi^2} = (1-6\xi) + \frac{2m_h^2}{m_\phi^2}(1-9\xi) - 18\xi\left(\frac{m_h^2}{m_\phi^2}\right)^2 = \frac{19}{18}(1-6.17105\xi) \quad (10)$$

Numerically, $g_{\phi hh}$ vanishes for $\xi = 0.162047$, *i.e.* very close to the value for which g_ϕ vanishes.

3. For the $VV = WW, ZZ$ couplings, the external $\eta_V = g_\phi - g_\phi^r \kappa_V$ values are:

$$\eta_V = g_\phi - g_\phi^r \kappa_V \simeq \ell\left[\kappa_V + 6\xi\left(\frac{m_h}{m_\phi}\right)^2 + 6\xi - 1\right], \quad (11)$$

where $\kappa_V = \frac{3kb_0 m_V^2}{2\Lambda_\phi^2 (k/M_{\rm Pl})^2} \simeq \frac{105 m_V^2}{m_1^{g\,2}}$ for $kb_0/2 \sim 35$ using the very good approximation $\Lambda_\phi(k/M_{\rm Pl}) = m_1^g$, see Eq. (8).

For $m_1^g = 3$ TeV, one finds $\kappa_W = 0.0761$ and $\kappa_Z = 0.0981$. As a result, η_V vanishes at $\xi = 0.150$, 0.146 in the W, Z cases, respectively. Of course, the η_V zeroes shift closer to the $\xi = 0.162$ point for $m_1^g = 5$ TeV, occurring at

$\xi = 0.158,\ 0.157$, respectively. The anomalous terms (not in figure) shift the WW, ZZ minima slightly.

4. Note that the g_ϕ, $g_{\phi hh}$ and non-κ_V term zeroes all approach the conformal point of $\xi = 1/6$ as $m_h/m_\phi \to 0$.

- **Resulting di-photon signal:**

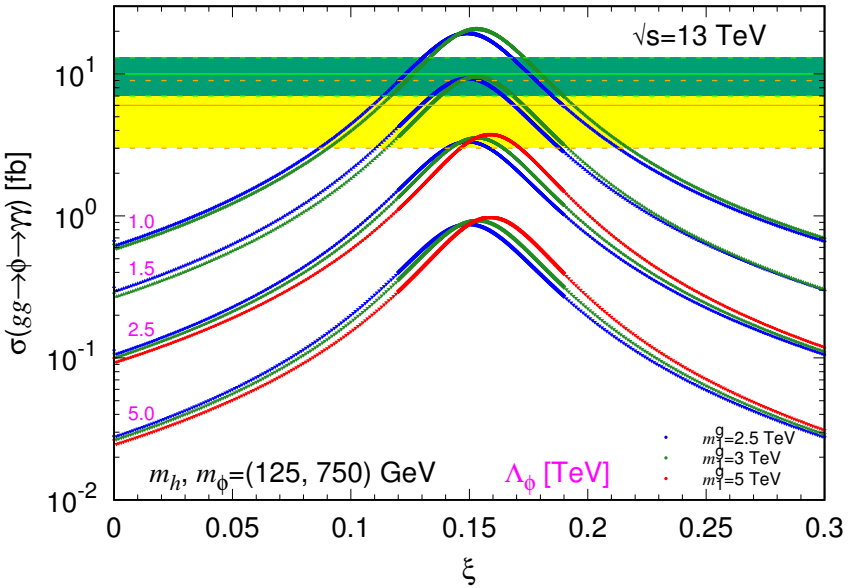

Figure 3: $\sigma(gg \to \phi \to \gamma\gamma)$ as a function of ξ for $m_h = 125$ GeV, $m_\phi = 750$ GeV and $m_1^g = 3$ TeV with different choices of Λ_ϕ as indicated by the coloration. ATLAS and CMS results are the light-green and yellow bands. Need $\Lambda_\phi = 1.5$ TeV to hit "central" values, which, in turn, is only possible if $m_1^g = 3$ TeV given $k/M_{\rm Pl} \leq 3$. Maximal $\gamma\gamma$ rate shifts from $\xi = 0.15$ to $\xi = 0.16$ for $m_1^g = 3$ TeV $\to 5$ TeV.

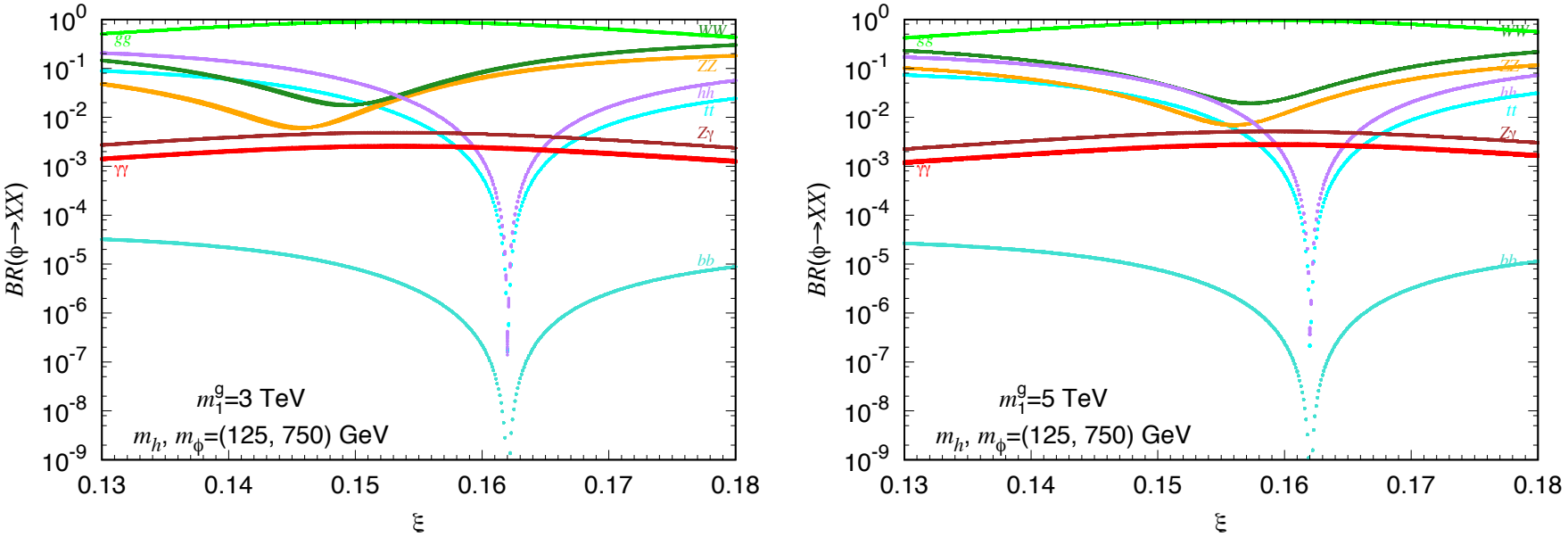

Figure 4: Branching ratios for the ϕ for $m_1^g = 3$ TeV and 5 TeV. The WW, ZZ minima shift towards $\xi = 0.162$ with increasing m_1^g. The maximal $\gamma\gamma$ rate is achieved for an intermediate value of ξ between the WW, ZZ minima and the $hh, t\bar{t}, b\bar{b}$ zeroes. Note that the WW, ZZ branching ratios do not vanish because of the extra non-SM tensor structure contributions related the the W, Z residing in the bulk.

A few important points:

- The suppression of all modes aside from $\gamma\gamma$, $Z\gamma$ and gg implies strong production and substantial $\gamma\gamma, Z\gamma$ rate, as well as limited constraints from all but the di-jet (gg) final state. More later using some benchmark points.
- **Clearly there are lots of rate correlations that will allow some intimate tests of the model, including determination of Λ_ϕ and m_1^g.**
- In the present one-doublet case, the h is **extremely** SM-like for the ξ values that give a strong $\gamma\gamma$ signal. But, multi-higgs on the brane is a possibility and then the $h125$ properties can deviate from those of the SM Higgs.
- From the plots of Fig. 5, we see that it is not possible to find a ξ choice such that $\mathrm{BR}(\phi \to \gamma\gamma) > \mathrm{BR}(\phi \to VV)$ for the values of m_1^g that allow Λ_ϕ such as to fit the data. Still, limits on all these final states from the 8 TeV data are consistent with both $m_1^g = 3$ TeV and $m_1^g = 5$ TeV.
- Indeed, we see that there is a rough lower bound on the VV final state branching ratios and so these should appear after sufficient data taking at 13 TeV.
- **The total width of the ϕ is predicted to be well below 1 GeV in this model. This seems to be preferred by CMS but not by ATLAS.**

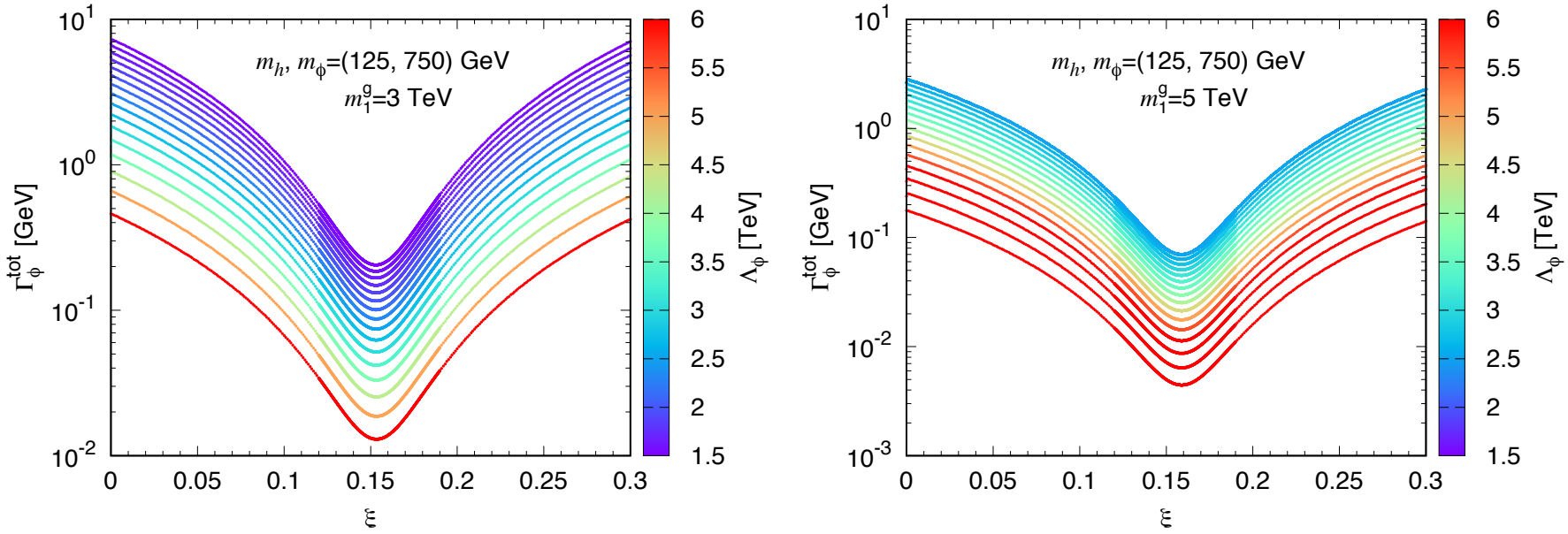

Figure 5: The total width of the radion $\Gamma^{\rm tot}{}_\phi$, as a function of ξ for $m_h = 125$ GeV, $m_\phi = 750$ GeV, $m_1^g = 3$ TeV (left) or $m_1^g = 5$ TeV (right) with different choices of Λ_ϕ.

– Of course, the gg final state always has very large branching ratio and should be detectable with future LHC running. Results for $gg \to \phi \to gg$ at 13 TeV are given in Fig. 6.

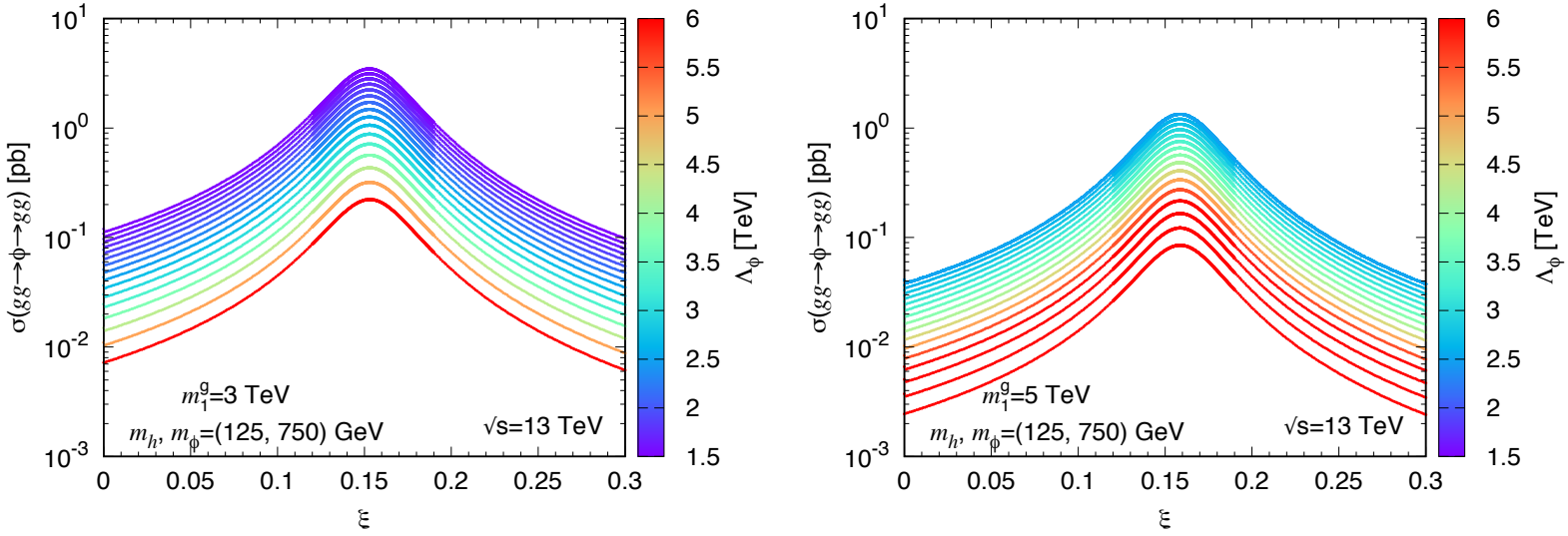

Figure 6: We plot $\sigma(gg \to \phi \to gg)$ as function of ξ for $m_h = 125$ GeV, $m_\phi = 750$ GeV and $m_1^g = 3$ TeV and 5 TeV, color-coded by Λ_ϕ.

For ξ values in the region around the peak for which the observed di-photon cross section is well described, one finds $1\text{pb} \lesssim \sigma(\text{gg} \to \phi \to \text{gg}) \lesssim 3$ pb.
This is certainly below the $10\ \text{pb}/\mathcal{A}$ bound extrapolated (using factor of 5 luminosity scaling) from the Run 1 limits assuming the same amount of integrated luminosity ($20\ \text{fb}^{-1}$).
However, for reasonable acceptance at the 13 TeV Run 2, the ATLAS and CMS collaborations should be able to see the gg signal in the di-photon excess region.

Table 1: Ten benchmark points for the Higgs-radion 750 GeV scenario interpretation of the di-photon excess at the LHC. Below Λ_ϕ is calculated for a given m_1^g and $k/M_{\rm Pl}$ according to Eq. (8). The dimensions for the dimensionful quantities are as follows: m_1^g [TeV], Λ_ϕ [TeV], ${\Gamma^{\rm tot}}_\phi$ [GeV], $\sigma_{gg}^{\phi}(VV, tt, hh)$ [fb] and σ_{gg}^{ϕ} (di-jet) [pb]. The cross sections are those at $\sqrt{s} = 13$ TeV.

BMP	m_1^g	ξ	Λ_ϕ	$k/M_{\rm Pl}$	$\mu_{gg}^{h}(\gamma\gamma)$	$\mu_{gg}^{h}(ZZ)$	$\mu_{WW}^{h}(ZZ)$
1	3	0.153	1.5	2	1.013	1.017	0.999
2	5	0.159	1.67	3	1.011	1.015	0.999
3	5	0.159	2.0	2.5	1.008	1.01	0.999
4	5	0.159	2.5	2	1.005	1.006	1.000
5	5	0.159	2.78	1.8	1.004	1.005	1.000
6	3	0.149	1.87	1.6	1.008	1.011	0.999
7	3	0.136	1.58	1.9	1.01	1.014	0.999
8	3	0.153	1.25	2.4	1.019	1.025	0.998
9	3	0.167	1.5	2.0	1.014	1.019	0.998
10	5	0.167	1.67	3.0	1.012	1.015	0.999

BMP	${\Gamma^{\rm tot}}_\phi$	$\sigma_{gg}^{\phi}(\gamma\gamma)$	$\sigma_{gg}^{\phi}({\rm di-jet})$	$\sigma_{gg}^{\phi}(ZZ)$	$\sigma_{gg}^{\phi}(WW)$	$\sigma_{gg}^{\phi}(Z\gamma)$	$\sigma_{gg}^{\phi}(t\bar{t})$	$\sigma_{gg}^{\phi}(hh)$
1	0.205	9.50	3.47	60.3	67.6	18.9	31.2	72.1
2	0.156	8.20	2.99	19.3	41.2	16.3	3.52	8.12
3	0.109	5.77	2.08	13.4	28.7	11.3	2.45	5.66
4	0.070	3.75	1.34	8.26	18.1	7.23	1.77	4.09
5	0.057	3.06	1.08	6.96	14.5	5.86	1.27	2.94
6	0.135	6.03	2.18	15.4	27.9	11.8	41.5	96.3
7	0.267	5.95	2.20	58.2	210	11.8	169	392
8	0.294	13.5	4.98	88.0	97.8	27.1	44.8	104
9	0.262	7.47	2.70	287	415	14.7	6.64	15.4
10	0.172	7.47	2.70	84.0	146	14.7	6.65	15.5

We now summarize important aspects of the BMPs.

- Point #1 gives the maximal gg-induced cross section in the $\phi \to \gamma\gamma$ (and, simultaneously, gg) final state for $m_1^g = 3$ TeV when $k/M_{\rm Pl} \leq 2$ is required. As noted above, this corresponds to $\Lambda_\phi = 1.5$ TeV. The maximum occurs at $\xi \sim 0.153$, *i.e.* part way between the minima for the WW, ZZ final state widths and $\xi \simeq 0.162$ where the $t\bar{t}, b\bar{b}, hh$ final state widths vanish. For this point the $\gamma\gamma$ final state has a cross section of order the central ATLAS value. Cross sections in the $hh, ZZ, WW, t\bar{t}$ final states (in that order) range from 72 fb down to 31 fb, while the gg final state has a cross section of 3.47 pb. $Z\gamma$ xsec of 19 fb converts to ~ 4 fb at 8 TeV, i.e. at the margin of < 3.9 fb.

- Points #2 — #5 illustrate results for $m_1^g = 5$ TeV. In this case, the maximal $\gamma\gamma$ cross section occurs at $\xi \sim 0.159$ (since the WW, ZZ cross section dips have moved closer to the $\xi \simeq 0.162$ point at which the $t\bar{t}, b\bar{b}, hh$ cross sections are zero). The different points illustrate results obtained for decreasing $k/M_{\rm Pl}$ values starting from the largest value allowed ($k/M_{\rm Pl} = 3$). Λ_ϕ ranges from 1.67 TeV up to 2.78 GeV, the latter being the value for which $\sigma(gg \to \phi \to \gamma\gamma)$ is at the lower edge of the CMS observation. Cross sections are ordered according to $WW > ZZ > Z\gamma > \gamma\gamma > hh > t\bar{t}$.

  The $\gamma\gamma$ cross section for BMP #2 is actually comparable to the case with

$m_1^g = 3$ TeV and $k/M_{\rm Pl} = 2$. This is due to the fact that the Λ_ϕ values corresponding to points #1 and #2 are very close in size. This is important, since if precision bounds or direct detection bounds push up the limits on m_1^g, this model can still reproduce the properties of the observed di-photon resonance at 750 GeV as observed by ATLAS.

- Comparing points #1 and #4 we observe the effects of increasing m_1^g from 3 to 5 TeV, keeping $k/M_{Pl} = 2$ constant (so that Λ_ϕ increases from 1.5 TeV to 2.5 TeV). As expected, we see a drop in the cross-sections to photons and gluons and in the total width.

- It is important to comment that BMPs #1 — #5 are easily consistent with the LHC 8 TeV data.

- Next, Points #6 and #7 are designed to show the limitation on how large the total width could be when fitting the central $\gamma\gamma$ rate reported by CMS. For the two points considered, we take $m_1^g = 3$ TeV. In these cases, the $\gamma\gamma$ final state cross section is smaller than that for any other final state mode, including the ZZ mode even though in the case of point #6 we have chosen ξ to be close to the ZZ minimum point.

For BMP #6, the total width is increased due to the increased width for the $t\bar{t}$ and hh final states. This is a result of choosing a ξ value that is well below the $\xi = 0.162$ value where the $t\bar{t}$ and hh modes are zero, see Fig. 5.

In the case of BMP #7 we have chosen an even lower value of ξ such that the WW and ZZ modes, as well as the $t\bar{t}$ and hh modes, all have large cross sections. In fact, Point #7 is excluded by existing 8 TeV limits on the hh channel (using a downwards rescaling factor of ~ 5 relative to the 13 TeV value given). This point thus illustrates the fact that one cannot describe the di-photon excess without having a total width well below 1 GeV.

- Point #8 is chosen to have a Λ_ϕ value (1.25 TeV) below our nominal lower limit of 1.5 TeV (which applies if $k/M_{\rm Pl} \leq 2$ and $m_1^g \geq 3$ TeV) in order to illustrate how we can obtain a $\gamma\gamma$ cross section at the upper limit of the ATLAS band. Still higher $\gamma\gamma$ cross sections are, of course, possible by lowering Λ_ϕ further. However, the ZZ final state cross section for this BMP #8 is already on the edge of the 8 TeV ATLAS exclusion limit (using a downwards rescaling factor of ~ 5 relative to the tabulated 13 TeV number).

- Points #9 and #10 are designed to illustrate results for ξ at the exact conformal point, $\xi = 1/6 \simeq 0.167$, with Λ_ϕ chosen so as to give a $\gamma\gamma$ cross section near

the center of the ATLAS+CMS band in the cases of $m_1^g = 3$ TeV and 5 TeV, respectively. The very large WW and ZZ cross sections in the $m_1^g = 3$ TeV case translate to $\sqrt{s} = 8$ TeV cross sections that exceed current limits. At $m_1^g = 5$ TeV, the WW and ZZ cross sections are large, but not in conflict with existing limits, although the ZZ final state prediction for 8 TeV is very close to the ATLAS exclusion limit. Thus, the conformal-limit choice for ξ is viable if m_1^g is large enough and Λ_ϕ is not much above 1.5 TeV.

Of course, these two points illustrate again the limitations on obtaining a large width for the 750 GeV radion state. In these cases we are making a ξ choice well above the minima of the ZZ and WW final state partial widths, but not so far above the zero of the hh partial width ($\xi = 0.162047$). Therefore (unlike for BMP #7 where the hh width is large) here it is the ZZ and WW final state exclusion limits that restrict our ability to get a total width that is more than a fraction of a GeV.

Important final state limits at 8 TeV.
Rescale upwards by $\times 5$ to compare to Table 1 entries.

final state	upper bound@8TeV	reference
di-jet	< 2.5 pb	[arXiv:1407.1376, CMS-PAS-EXO-14-005]
$t\bar{t}$	< 300 fb	[arXiv:1309.2030]
hh	< 36 fb	[arXiv:1509.04670]
WW	< 38 fb	[arXiv:1509.00389, arXiv:1504.00936]
ZZ	< 17 fb	[arXiv:1507.05930]
$Z\gamma$	< 4 fb	[arXiv:1407.8150]

Conclusions

- The Higgs responsible for EWSB has emerged and is really very SM-like.
- RS avoids hierarchy problem and so maybe no supersymmetry. RS requires a radion, the quantum fluctation association with brane separation.
- Have we seen the radion at 750 GeV? It is very consistent with what is seen in the $\gamma\gamma$ mode and absence (so far) of other modes if $\Lambda_\phi \lesssim 2.5$ TeV.
- RS scenario can be extended by allowing more complicated Higgs sector on the brane. Thus, there is no reason not to have additional Higgs bosons.

  One can just add to the Higgs sector of the model with impunity so long as the TeV brane multi-higgs model parameters are chosen so that we are in the alignment limit for whatever Higgs boson has mass of 125 GeV.

  Of course, the $g_\phi \sim 0$ limit is needed to prevent dilution of the $\phi \to \gamma\gamma$ signal rate.

  We must continue to push hard to improve limits/sensitivity to additional Higgs bosons.

- Higgs could be everything, even providing the dark matter.

  This is much easier/less-constrained in the 2HDM + Singlet context than in the SM + Singlet context because either h or H can be the SM-like Higgs at 125 GeV while the other, H or h, respectively, can mediate dark matter annihilation.